

Shape deformation of embedded metal nanoparticles by swift heavy ion irradiation

Fouran Singh¹, S. Mohapatra¹, J. P. Stoquert², D. K. Avasthi¹, J. C. Pivin³

¹Materials Science Group, Inter University Accelerator Centre, Aruna Asaf Ali Marg, New Delhi 110067, INDIA; ²Laboratoire INESS, BP20, 67037 Strasbourg Cedex 2, FRANCE; ³CSNSM-IN2P3, Orsay Campus, FRANCE

ABSTRACT

Swift heavy ions (SHI) induce high densities of electronic excitations in narrow cylindrical volumes around their path. These excitations have been used to manipulate the size and shape of noble metal nanoparticles embedded in silica matrix. Films containing noble metal nanoparticles were prepared by magnetron co-sputtering techniques. SHI irradiation of films resulted in the formation of prolate Ag nanoparticles with major axis along the ion beam direction. It has been observed that the nanoparticles smaller than the track size dissolve and other grow at their expense, while the nanoparticles larger than track size show deformation with major axis along the ion beam direction. The aspect ratio of elongated nanoparticles is found to be the function of electronic energy loss and ion fluence. Present report will focus on the role of size and volume fraction on the shape deformation of noble metal nanoparticles by electronic excitation induced by SHI irradiation. The detailed results concerning irradiation effects in silica-metal composites for dissolution, growth and shape deformation will be discussed in the framework of thermal spike model.

Key words: Nanoparticles, electronic excitations, swift heavy ions, shape deformation, TEM, thermal spike.

PACS: 78.67.Bf, 61.80.-x, 65.80.+n, 79.20.Rf

1. INTRODUCTION

The confinement of light is a very important and current challenge for nano-dimensional integrated optical devices, near-field optics and nanophotonics. Noble metal nanoparticles are attractive in this field because of their surface plasmon resonance (SPR), which couples with electromagnetic fields and leads to interesting properties such as a transmission in a selected wavelength range [1], a nonlinear optical response [2], and a highly localized field enhancement [3,4]. Therefore, noble metal particles have great potentials as elements of biosensor [5], nanophotonic devices [6,7], and plasmonic devices [8]. These with anisotropic shapes are interesting because their polarizability depends on the filed orientation. For large aspect ratios, plasmon band may shift well into the infrared along the major axis, making the particles useful for telecommunication applications. In addition, anisotropic particles show a reduced plasmon resonance time and longer dephasing time as compared to spherical particles. The particle size, shape or spatial distribution can be modified by thermal annealing [9], ion irradiation [10-12] and laser treatment [9,13,14]. Swift heavy ion (SHI) irradiation of amorphous materials leads to an anisotropic deformation, known under the name of hammering.

In a study of SHI effects on silica colloidal particles encapsulating cores of Au (with smaller sizes), it has been found that the silica shells expanded perpendicular to the ion beam direction and compressed parallel to the beam, becoming oblate ellipsoids. On the contrary, the Au core underwent an elongation parallel to the ion beam by a creep process, because they are heated and compress by the matrix at same time [15]. In another study on ion-exchanged glasses containing Ag nanoparticles with a filling factor of a few % and sizes of 5-10 nm, SHI induced an alignment of the particles [16]. In the

present paper we are reporting a change in shape from spherical to ellipsoidal by electronic excitations induced by heavy ion irradiation at lower ion fluences. This is the detailed report using transmission electron microscopy (TEM) on the elongation of silver nanoparticles in contradiction to the work of Penninkhof et al [17] that embedded silver particles cannot be elongated like Au nanoparticles [17,18], but in accordance with work of Oliver et al [19].

2. EXPERIMENTAL DETAILS

Silica films containing silver nanoparticles with a volume fraction of 3-6 at. % were grown by magnetron co-sputtering on silicon substrates. The as-deposited films were annealed at 950 °C for 1 hour under Ar+H₂ (5%) in a continuous flow tubular furnace for growing particles without oxidation. Annealed samples were irradiated, using 15UD Tandem Pelletron accelerator at Inter University Accelerator Centre (IUAC), New Delhi, with 120 MeV Au ions in high vacuum chamber with a base pressure of 3.2×10^{-6} torr. The beam current was kept constant ~ 0.5 pna (particle nano ampere) during the irradiation. These ions loose 13.91 and 33.53 keV/nm in electronic excitations in silica and silver respectively, as determined from SRIM code. The samples were irradiated with an ion beam 45° off normal at fluence of 3×10^{13} ions/cm². Cross sectional TEM investigations were carried out using JEOL 2010 UHRTEM facility at Institute of Physics, Bhubaneswar.

3. RESULTS

Fig. 1(a) shows the TEM micrograph of silver nanoparticles after annealing at 950 °C and the corresponding histogram of sizes is shown in Fig. 1(b). They clearly reveal that the particles are spherical with a narrow size distribution of particles. The mean particle size and size straggling calculated by fitting the data with a Gaussian distribution are (9.6 ± 1.5) nm. The inset of Fig. 1(a) also shows a high-resolution micrograph of a particle, evidencing its crystallinity and the measured lattice parameter, of 0.206 nm, corresponds to the (002) spacing of fcc Ag. A change from spherical to ellipsoidal shape of the silver nanoparticles is observed after irradiation, with the long axis of the ellipsoids aligned along the ion beam direction, as shown in Fig. 2(a) for the irradiation fluence of 3×10^{13} ions/cm². The high resolution TEM micrograph of Fig. 2(b) shows that the particles remain crystalline with a lattice parameter of about 0.212 nm (the arrow in the image indicates the direction of ion beam, perpendicular to the film surface). The mean particle size for this fluence of 120 MeV Au ions is 13.9 ± 1.7 nm along the major axis and 9.4 ± 1.7 nm along the minor axis, as determined from histograms of size shown in Figs. 2(c) and (d), and their average aspect ratio is about 1.47. Further, the comparison of histograms in Figs. 1 and 2 also puts into evidence that the smallest particles disappear after ion irradiation, while the mean size of nanoparticles increases. This result seems to indicate that the electronic excitations induce the dissolution of nanoparticles smaller than the ion track in silica (of which diameter will be specified latter) whereas larger ones grow and get elongated along the beam direction in accordance with previous works on other systems [18-22].

4. DISCUSSION

The mechanism of the observed shape changes can be explained by the high density of electronic excitations induced by SHI, of which energy is transmitted to the lattice by several processes [23]: Coulomb explosions [24,25], thermal spikes [26,27] and hammering [28,29]. The preponderance of each one depends on the electronic structure and is a subject of discussion, especially in the case of composite systems. Coulomb explosions occur mainly in insulators, due to the ejection of secondary electrons with high energies out of the core of each ion track (cylindrical volume with a radius of a few nm). However, most of the authors consider that the agitation of target atoms by electron phonon coupling is more significant, as it lasts for a longer time than electrical perturbations and takes place in targets of any nature [27]. The calculations of thermal exchanges between the electronic and atomic systems during these pseudo-thermal spikes have been used to explain the differences of radiation resistance of metal, semiconductors and ionic insulators [30]. The solution of equations for targets made of a matrix embedding an isolated particle is expected to put into evidence a phenomenon of transient overheating of the particle, if it is a better conductor of heat than the matrix.

A. Simulations

Simulations of thermal spikes for a system with a single particle at the origin at coordinates (of cylindrical type r, y as shown in Fig. 3) were performed by solving the following coupled differential equations, which describes the temperature evolution in the electronic and atomic subsystems of the materials [26,31]:

$$C_e \rho \frac{\partial T_e(\vec{r}, t)}{\partial t} = \vec{\nabla} \cdot (K_e \overline{\nabla T_e(\vec{r}, t)}) - g(T_e - T_a) + A(\vec{r}, t)$$

$$C_a \rho \frac{\partial T_a(\vec{r}, t)}{\partial t} = \vec{\nabla} \cdot (K_a \vec{\nabla} T_a(\vec{r}, t)) + g(T_e - T_a)$$

Where, C_e , K_e and T_e are the specific heat, thermal conductivity and temperature of electronic subsystem, while C_a , K_a and T_a are the specific heat, thermal conductivity and temperature of the atomic subsystem. ρ is the mass density of the lattice and g is the electron-phonon coupling constant. $A(r,t)$ is the energy density per unit time provided by the incident ions to the electronic subsystem at radius r and time t . Heat transfers from the electrons to the lattice via electron-phonon coupling and propagates simultaneously in the different subsystems.

Fig. 3(a) shows the temporal profile of temperature at the center of silver metal particles with different sizes of 2 to 30 nm embedded in silica, crossed by energetic ions along their diameters. Values of the parameters used in the calculations are summarized in Table 1. The parameters for silver are based on reference [26], while for silica is based on reference [32]. Results of the simulations show that nanoparticles up to a diameter of 10 nm only are in melt phase, while the particles bigger than 10 nm can not be melted. Fig. 3(b) represents the radial temperature profile in the $y=0$ plane of the nanoparticles after 100 ps, which is the time of the order of electron-phonon coupling. From the melting and boiling temperatures T_m and T_b and temperature spatial profiles of Fig. 3, one can conclude that a cylinder of 7.4 nm in diameter is melted in the matrix and small particles under a strong overheating over T_m on same diameter. It is known that the melting temperature of metal nanoparticles is usually lower than that of bulk metal. Introducing in the calculations the estimated values of T_m for free Ag particles given in [33] neither modify significantly the maximum temperature reached in the nanoparticles nor the temporal and spatial gradients presented in Fig. 3. The same remark is valid for

the electron-phonon coupling constant which is not precisely known for the nanoparticles. Varying this constant by one order of magnitude in the input does not severely affect the simulation results and conclusions.

B. Interpretation

On basis of these simulations, the irradiation induced nanostructures modifications can be explained by two different effects:

a) The nanoparticles with diameters up to 6 nm get completely melted and dissolved in the melted cylinder of silica, because of their strong overheating. Their temperature reaches T_b of silver; so that the Ag atoms become very mobile. The total volume of metal phase after freezing remains almost constant because Ag is little soluble in silica. The dissolved Ag atoms contribute to the growth of particles having diameters larger than 6 nm (note that this ripening process cannot be called Ostwald ripening since it does not proceeds from a gradient of chemical potential). For explaining more clearly the anisotropic diffusion of Ag atoms in a molten phase, we have plotted in Fig. 4(a) the temporal profile of temperature at different (y, r) coordinates (defined by schemes) for particles of diameter 6 nm.

b) The nanoparticles with diameters in the range of 8-10 nm are also in molten state during the time interval 50-500 ps, but their temperature remains close to T_m . This is illustrated by the temporal profile of temperature at different (y, r) coordinates for particles of 10 nm in Fig. 4(b). The temperature in the silica track is larger than the temperature in the centre of nanoparticles. However, due to the differences in the volume expansion and compressibility a large pressure is expected in the molten silver particles,

which induces a creep deformation i.e. the elongation of particles along the ion beam direction.

The results of these simulations based on thermal spike model are in coherence with our experimental observation from TEM. One could argue that the elongation of the particles may also be explained by the hammering of the matrix, if particles of all sizes became elongated. But in present case the proportion of small particles decreases and the few ones observed in the images remain spherical.

5. CONCLUSION

Electronic excitations in tracks by 120 MeV Au ions induce an elongation of silver nanoparticles with a relatively low volume fraction and slightly larger size than the tracks in the matrix. Simulations based on the thermal spike model help to explain why particles up to the diameter of tracks in the matrix disappear, while those with larger diameters grow at their expenses. Nanoparticles with diameter 8-10 nm get elongated along the beam direction.

Acknowledgements

Authors are thankful to Dr. P.V. Satyam from IOP Bhubaneswar for extending his HRTEM facility. One of the author (FS) is thankful for department of Science and technology (DST) for providing the travel support and Director IUAC for providing local expenses for presenting this invited paper in SHIM2008 conference in Lyon, France.

Reference:

- [1] T. W. Ebbesen, H. J. Lezec, H. F. Ghaemi, T. Thio and P. A. Wolff, *Nature* 391 (1998) 667.
- [2] V. M. Shalaev, *Optical Properties of Nanostructured Random Media* (Springer-Verlag, Berlin, 2002).
- [3] C. Bohren and D. Huffman, *Absorption and Scattering of Light by Small Particles* (Wiley, New York, 1983).
- [4] U. Kreibig and M. Vollmer, *Optical Properties of Metal Clusters* (Springer-Verlag, Berlin, 1995).
- [5] D. A. Schultz, *Curr. Opin. Biotechnol.* 14 (2003) 13.
- [6] M. Ohtsu, K. Kobayashi, T. Kawazoe, S. Sangu and T. Yatsui, *IEEE J. Sel. Top. Quantum Electron.* 8 (2002) 839.
- [7] P. N. Prasad, *Nanophotonics* (Wiley, Hoboken, NJ, 2004).
- [8] S. A. Maier, M. L. Brongersma, P. G. Kik, S. Meltzer, A. A. G. Requicha and H. A. Atwater, *Adv. Mater.* 13 (2001) 1501.
- [9] R. A. Wood, P. D. Townsend, N. D. Skelland, D. E. Hole, J. Barton and C. N. Afonso, *J. Appl. Phys.* 74 (1993) 5754.
- [10] J. C. Pivin, M. A. Garcia, H. Hofmeister, A. Martucci, M. Sendova-Vassileva, M. Nikolaeva, O. Kaitasov and J. Llopis, *Eur. Phys. J. D* 20 (2002) 251.
- [11] F. Gonella, G. Mattei, P. Mazzoldi, E. Cattaruzza, G. M. Arnold, G. Battaglin, P. Calvelli, R. Polloni, R. Bertonecello and Jr. R. F. Haglund, *Appl. Phys. Lett.* 69 (1996) 3101.

- [12] J. C. Pivin, G. Roger, M. A. Garcia, F. Singh and D. K. Avasthi, Nucl. Instr. and Meth. B 215 (2004) 373.
- [13] L. Stepanov, D. E. Hole and P. D. Townsend, Nucl. Instru. Meth. B 166-167 (2000) 882.
- [14] M. Sendova, M. Sendova-Vassileva, J. C. Pivin, H. Hofmeister, K. Coffey and A. Warren, J. Nanoscience and Nanotech. 6 (2006) 748.
- [15] S. Roorda, T. van Dillen, A. Polman, C. Graf, A. van Blaaderen and B. J. Kooi, J Adv. Mater. 16 (2004) 235.
- [16] J. J. Penninkhof, A. Polman, A. Sweatlock Luke, A. Maier Stefen, A. Atwater Harry, A. M. Vredenberg and B. J. Kooi, Appl. Phys. Lett. 83 (2003) 4137.
- [17] J.J. Penninkhof, T. van Dillen, S. Roorda, C. Graf, A. van Blaaderen, A. M. Vredenberg, and A. Polman, Nucl. Instru. Meth. B 242 (2006) 523.
- [18] Y. K. Mishra, F. Singh., D. K. Avasthi, J. C. Pivin, D. Malinovska, E. Pippel, Appl. Phys. Lett. 91 (2007) 063103.
- [19] A. Oliver, J. A. Reyes-Esqueda, J. C. Cheang-Wong, C. E. Román-Velázquez, A. Crespo-Sosa, L. Rodríguez-Fernández, J. A. Seman, and Cecilia Noguez Phys. Rev. B 74 (2006) 245425.
- [20] E. Valentin, H. Bernas, C. Ricolleau and F. Creuzet, Phys. Rev. Lett. 86 (2001) 99.
- [21] Y. K. Mishra, D. K. Avasthi, P. K. Kulriya, F. Singh, D. Kabiraj, A. Tripathi, J. C. Pivin, I. S. Bayer and A. Biswas, Appl. Phys. Lett. 90 (2007) 073110.
- [22] D' Orleans C, Stoquert J P, Estournès C, Cerruti C, Grob J J, Guille J L, Haas F, Muller D and M. Richard-Plouet, Phys. Rev. B 67 (2003) 220101R.
- [23] L. T. Chadderton, Rad. Measurements 36 (2003) 13.

- [24] R. L. Fleischer, P. B. Brice and R. M. Walker, *J. Appl. Phys.* 36 (1965) 3645.
- [25] D. Lesueur and A. Dunlop, *Rad. Eff. Def. Solids* 126 (1993) 163.
- [26] Z. G. Wang, C. Dufour, E. Paumier, and M. Toulemonde, *J. Phys. Condens. Matter.* 6 (1994) 6733.
- [27] Meftah, J. M. Costantini, N. Khalfaoui, S. Boudjadar, J. P. Stoquert, F. Studer and M. Toulemonde, *Nucl. Instru. Meth. B* 237 (2005) 563.
- [28] Ming-Dong Hou, S. Klaumunzer and G. Schumacher, *Phys. Rev. B* 41 (1990) 1144.
- [29] H. Trinkaus and A. I. Ryazanov, *Phys. Rev. Lett.* 74 (1995) 5072.
- [30] Benyagoub, S. Klaumunzer, L. Thome, J. C. Dran, F. Garrido and A. Dunlop, *Nucl. Instru. Meth. B* 64 (1992) 684.
- [31] M. Lifshitz, M. I. Kaganov and L. V. Taratanov, *J. Nucl. Energ. Parts A/B* 12 (1960) 69.
- [32] M. Toulemonde, *Private communication*.
- [33] T. Castro, R. Reifenber, E. Choi and R. P. Andres, *Phys. Rev. B* 42 (1990) 8548.

TABLE I. Parameters and values of constants used in the thermal spike calculations

	Atoms		Electrons	
	Ag	a-SiO ₂	Ag	SiO ₂
Density ρ (g.cm ⁻³)	10.5	2.2		
Specific heat C (J.g ⁻¹ .K ⁻¹)	0.25-6.8 .10 ⁻⁵ T _a + 6.5 x10 ⁻⁹ T _a ² ; 300<T _a <1235	3.297 x10 ⁻⁴ T _a +0.65 300<T _a <1972		
ρC (Jcm ⁻³ K ⁻¹)	0.28	-3 x10 ⁻⁸ T _a +1.3	63 x 10 ⁻⁶ T _e ; T _e <19400K	1
Thermal conductivity K (Wcm ⁻¹ K ⁻¹)	3.5+0.0034T _a -3.9e-6T _a ² 300<T _a <1972	1.00 x10 ⁻³		1.21 ; T _e >19400K
g (Wcm ⁻³ K ⁻¹)	1.2			
Latent heat of fusion (Jg ⁻¹)	104.6	142	1.30 x10 ¹²	1.25 x10 ¹³
Latent heat of vaporization (Jg ⁻¹)	2096.8	4715		
Temperature of melting (K)	1235	1972		
Temperature of boiling (K)	2485			

Figure captions:

Figure 1. (a) Cross sectional TEM micrograph of pristine silica film containing silver nanoparticles (Inset shows the HRTEM image of one nanoparticle). (b) Histogram of particles size distribution. Dashed line shows the Gaussian fit to size distribution.

Figure 2. (a) Cross sectional TEM micrograph of 120 MeV Au irradiated silica film containing silver nanoparticles for a fluence of 3×10^{13} ions/cm²; (b) HRTEM image of deformed particle and arrow shows the direction of beam; (c) histograms of size distribution for major axes and (d) for minor axes of deformed particles. Dashed line shows the Gaussian fit to the size distributions.

Figure 3. (a) Temporal profile of temperature in the centre of nanoparticles (diameters between 2-30 nm) crossed by energetic ions. T_m and T_b are the melting and boiling temperature of bulk silver and silica. (b) Radial profile of temperature in the $y=0$ plane of nanoparticles after 100 ps. Inset shows coordinates (y , r) in reference of direction of ion beam. $T(r)$ is the radial profile of temperature and R_T is the track radius in silica.

Figure 4. Temporal profile of temperature at different (y , r) coordinates from the centre of (a) 6 nm and (b) 10 nm nanoparticles. Insets in each plot indicate the (y , r) coordinates in reference to the centre of nanoparticles (bigger circle for the nanoparticle, smaller symbols for coordinates).

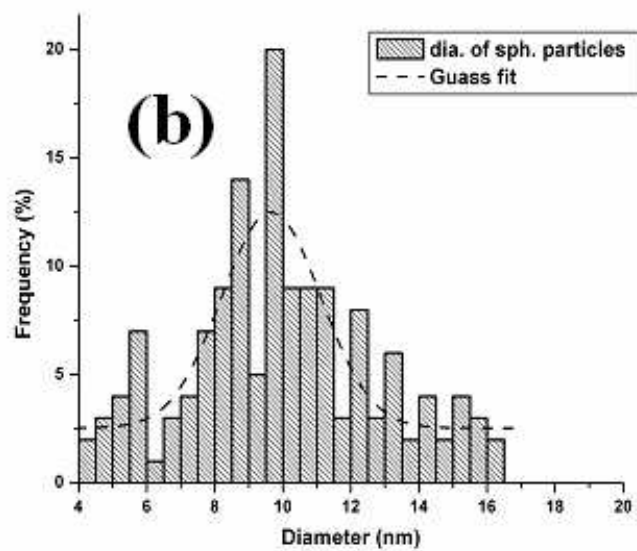
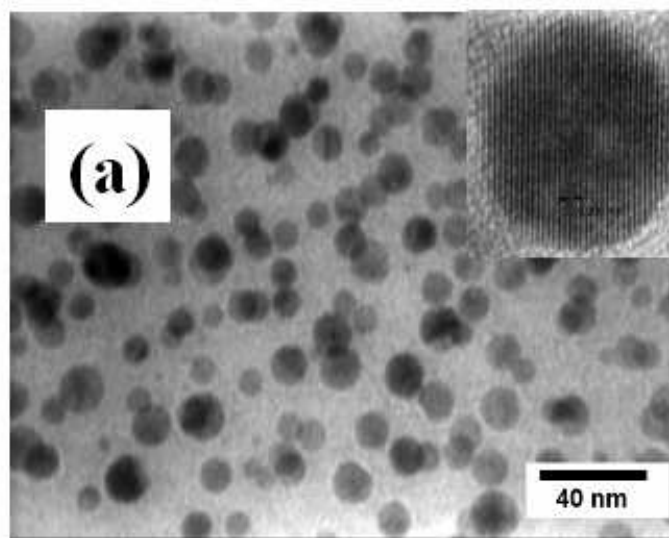


Figure 1

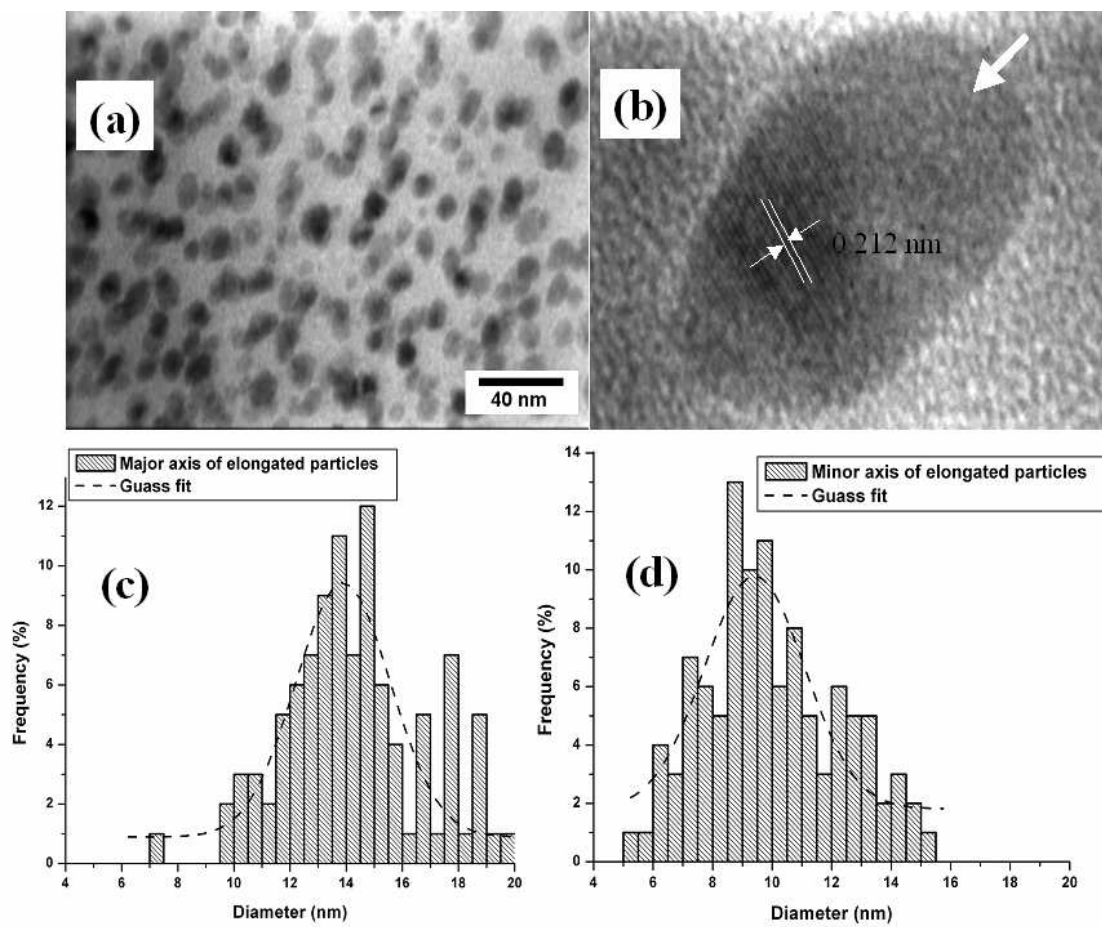


Figure 2

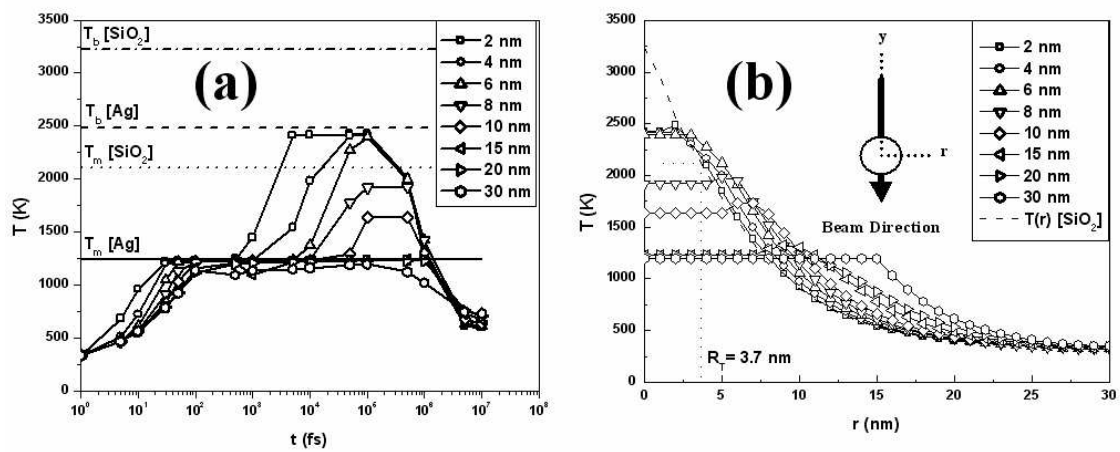


Figure 3

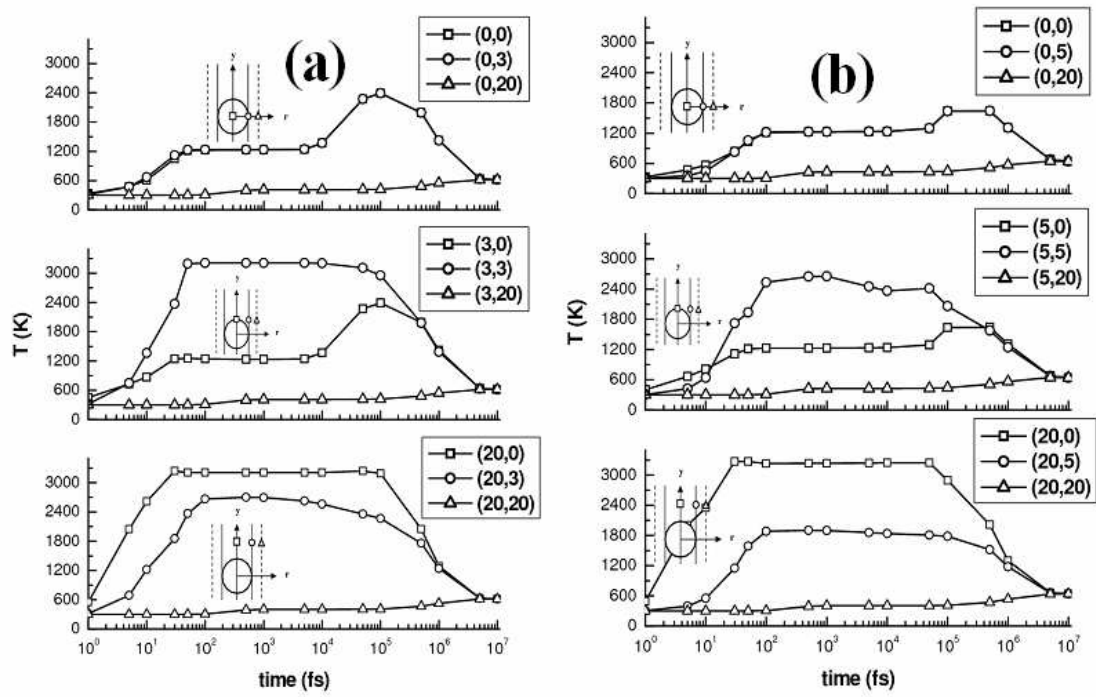


Figure 4